

The dynamics of double slab subduction

A.F. Holt,^{1,2} L.H. Royden¹ and T.W. Becker³

¹*Department of Earth Atmospheric and Planetary Science, MIT, Cambridge, MA 02139, USA. E-mail: adamholt@mit.edu*

²*Department of Earth Sciences, University of Southern California, Los Angeles, CA 90089, USA*

³*Jackson School of Geosciences, The University of Texas, Austin, TX 78758, USA*

Accepted 2017 January 3. Received 2016 December 29; in original form 2016 October 5

SUMMARY

We use numerical models to investigate the dynamics of two interacting slabs with parallel trenches. Cases considered are: a single slab reference, outward dipping slabs (out-dip), inward dipping slabs (in-dip) and slabs dipping in the same direction (same-dip). Where trenches converge over time (same-dip and out-dip systems), large positive dynamic pressures in the asthenosphere are generated beneath the middle plate and large trench-normal extensional forces are transmitted through the middle plate. This results in slabs that dip away from the middle plate at depth, independent of trench geometry. The single slab, the front slab in the same-dip case and both out-dip slabs undergo trench retreat and exhibit stable subduction. However, slabs within the other double subduction systems tend to completely overturn at the base of the upper mantle, and exhibit either trench advance (rear slab in same-dip), or near-stationary trenches (in-dip). For all slabs, the net slab-normal dynamic pressure at 330 km depth is nearly equal to the slab-normal force induced by slab buoyancy. For double subduction, the net outward force on the slabs due to dynamic pressure from the asthenosphere is effectively counterbalanced by the net extensional force transmitted through the middle plate. Thus, dynamic pressure at depth, interplate coupling and lithospheric stresses are closely linked and their effects cannot be isolated. Our results provide insights into both the temporal evolution of double slab systems on Earth and, more generally, how the various components of subduction systems, from mantle flow/pressure to interplate coupling, are dynamically linked.

Key words: Mantle processes; Subduction zone processes; Dynamics of lithosphere and mantle; Kinematics of crustal and mantle deformation.

1 INTRODUCTION

Regional interactions between multiple subducting slabs have been invoked to explain enigmatic slab kinematics at a number of subduction zones, past and present. Pertinent examples include the rapid pre-collisional convergence between India and Eurasia, and the advancing motion of the Izu-Bonin trench (e.g. Carlson & Melia 1984; Čížková & Bina 2015; Jagoutz *et al.* 2015). Such non-standard slab kinematics are not typically observed in time-dependent numerical models that consider single slab subduction (e.g. Funicello *et al.* 2003; Enns *et al.* 2005; Stegman *et al.* 2006). In order to understand the dynamic origins of such kinematics, we use time-dependent, 3-D numerical models of double slab subduction (i.e. slabs/trenches within a few thousand kilometres of each other) to isolate the first-order dynamic processes at work in double slab subduction systems. We systematically investigate how, and the degree to which, the presence of an additional subduction slab, with a range of slab dip directions, modifies subduction dynamics.

The study of multi-slab systems is particularly suited to understanding how slabs interact with the asthenosphere and surface plates because they extend the range of asthenospheric pressure, slab dip and plate coupling forces beyond those found in single slab systems, thus providing additional insight into the dominant controls on subduction dynamics. This study focuses on three basic double slab geometries, involving simultaneous subduction along two parallel trench systems of equal length (Fig. 1). The slabs interact with one another through viscous stresses induced by asthenospheric flow and by stresses transmitted from trench to trench along the intervening plate.

We show that there are simple connections between the various components of the subduction system that govern the slab's dynamic evolution. Such a physical understanding of how slabs 'talk' to each other is important to unravel how double slab systems evolve, and may on occasion explain observed slab kinematics more consistently than treating slabs in isolation. More importantly, analysis of multi-slab systems does not merely introduce added

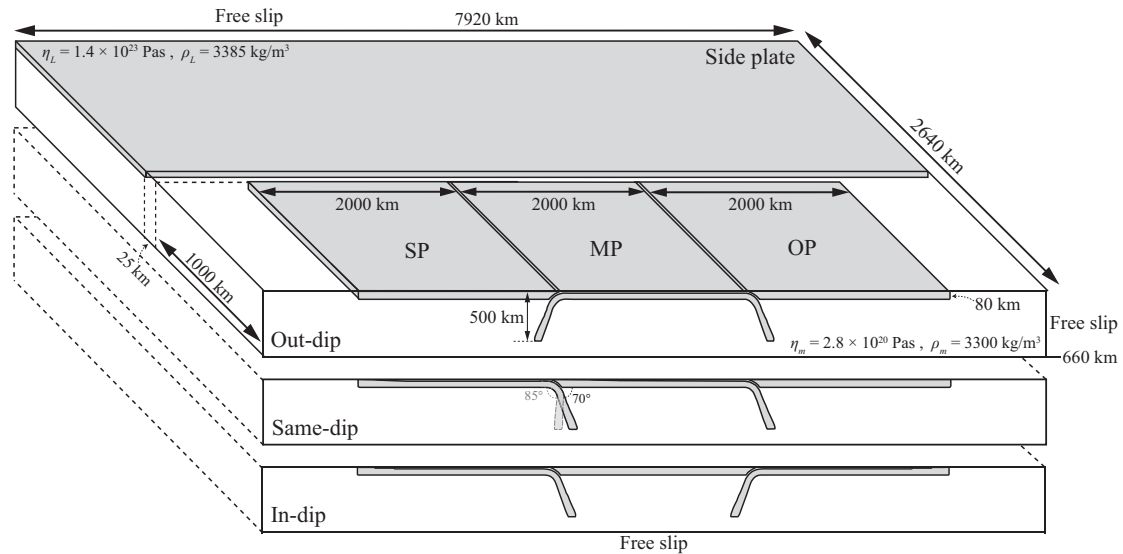


Figure 1. Illustration of the initial conditions for numerical, double slab subduction models. Key physical parameters are illustrated on the upper, same-dip polarity schematic. All models have a plane of symmetry in the trench-perpendicular direction. The out-dip and in-dip configurations have an additional plane of symmetry in the trench-parallel direction.

complexity, but provides additional insights into the dynamics of a single slab.

2 PREVIOUS SUBDUCTION MODELING STUDIES

Subduction has been modeled extensively with numerical and analogue techniques (e.g. Becker *et al.* 1999; Funicello *et al.* 2003; Kincaid & Griffiths 2003; Enns *et al.* 2005; Stegman *et al.* 2006), and a more limited number of analytical studies (e.g. England & Wikins 2004; Royden & Husson 2006; Jagoutz *et al.* 2015). The reduction in gravitational potential energy as a denser slab descends into the asthenosphere provides the energy needed to drive viscous flow within the surrounding asthenosphere. In conjunction with plate bending and plate coupling at the subduction interface, these processes act to determine subduction rate (e.g. Conrad & Hager 1999; Bellahsen *et al.* 2005). Because all of these processes operate together within a single dynamic system, the subduction process is best understood without prescribing any part of the kinematics or geometry such as dip, that is, through the use of fully dynamic models.

There are several factors that have been found to strongly affect subducting slab shapes and kinematics, including slab buoyancy, slab width, plate size and lithosphere/asthenosphere rheology. Thus, most modeling studies are focused on elucidating the behaviour of a single slab, so that results can readily be compared to natural systems. However, such comparisons of observed and predicted convergence rate, slab dip, or trench motions indicate that our understanding of subduction is incomplete (e.g. Becker & Faccenna 2009; Billen 2009).

3-D, single slab studies have proven useful for illuminating the role of toroidal flow of asthenosphere around the slab as it advances or retreats through the mantle, and the associated impact of the third dimension (e.g. plate/trench width) on slab kinematics (e.g. Funicello *et al.* 2003; Schellart 2004; Funicello *et al.* 2006; Piro-mallo *et al.* 2006; Royden & Husson 2006; Stegman *et al.* 2006). While these works neglect the presence of the upper plate, recent studies consider 3-D subduction dynamics in a two-plate system

(e.g. Yamato *et al.* 2009; Duarte *et al.* 2013; Schellart & Moresi 2013), a feature required to model the relevant force transmission in double slab subduction. The three-dimensionality of asthenospheric flow is even more important in the multi-slab subduction systems considered, because trench-parallel asthenospheric flow is required to enable relative trench motion (Fig. 1). As explored in the subsequent sections, this produces important differences in the asthenospheric velocity field, dynamic pressure distribution and inter- and intraplate stress, relative to single slab subduction.

Previous numerical models of double subduction typically omit the overriding plates (e.g. Di Leo *et al.* 2014), consider a limited duration (0.1 Myr) of time-evolving subduction (e.g. Lin & Kuo 2016), or restrict the model domain to 2-D (e.g. Mishin *et al.* 2008; Čížková & Bina 2015). In the 2-D simulations, convergent motion between the slabs requires the asthenosphere between the slabs to flow downward into the more viscous lower mantle. Such 2-D models have elucidated the wide range of plate kinematics associated with double subduction (e.g. trench advance; Čížková & Bina 2015). However, lateral flow confinement affects trench motion systematics (e.g. Enns *et al.* 2005), and, in certain cases, 2-D double slab setups have resulted counterintuitive processes such as e-duction (the opposite of subduction), which is not observed in the geological record (Mishin *et al.* 2008). The recent study of Király *et al.* (2016) uses 3-D numerical models to highlight how neighbouring slabs (i.e. in trench-parallel direction) can affect each other's evolution within a threshold distance of ~ 600 km. In this trench-parallel configuration, the slabs interact via viscous stresses induced by mantle flow. Here, we study slabs that interact in the trench-perpendicular direction, where stresses are transmitted directly through the intervening plate can also play a role.

3 METHODS

We use the finite-element code CitcomCU (Moresi & Gurnis 1996; Zhong 2006) to model incompressible Stokes flow in a 3-D, Cartesian domain with Newtonian viscosity, in an approach similar to Holt *et al.* (2017) but without the inclusion of a stress-dependent rheology. Here, we use purely viscous subduction models in order

to elucidate the fundamental processes associated with double slab subduction in 3-D. We use a density and viscosity field that is dependent purely on composition (e.g. Enns *et al.* 2005). We consider the omission of thermal effects to be a reasonable simplification because thermal slabs are thought to be generally coherent even within the lower mantle (e.g. Tan *et al.* 2002). We initially place 40 tracers within each of the elements and the compositional field is advected using tracer particles (e.g. McNamara & Zhong 2004). Separate sets of tracers are used to define the lithospheric plates, and the weak ‘crustal’ layers embedded within the subducting plates. We use an asthenospheric viscosity of 2.8×10^{20} Pa s and density of 3300 kg m^{-3} . The plates have a uniform density of 3385 kg m^{-3} . This thickness and density of the lithosphere provides negative buoyancy, relative to the asthenosphere, that is comparable to that of old oceanic plates. The asthenosphere viscosity was chosen to yield a steady-state subduction rate of $\sim 7 \text{ cm yr}^{-1}$ for single slabs, comparable to the subduction rates observed for old oceanic lithosphere. (For a purely viscous rheology, the asthenospheric viscosity and the lithosphere–asthenosphere density contrast trade-off via the Stokes velocity scaling ($\sim \Delta\rho/\eta$), which dictates subduction rate).

The finite-element sizes vary from 6 km in regions that are in the upper 200 km of the domain and proximal to the trench, to 14 km elsewhere. We have conducted resolution tests using 2-D setups of both our single and our out-dip double subduction model. We find that reducing the element size by factors of 2 and 4 (in all directions) results in <3 per cent variability in average convergence rate, equivalent slab morphologies and nearly identical dynamic pressure profiles.

For the Q_1 – P_0 elements used in CitcomCU, checkerboard modes can occur within the pressure field (e.g. Gresho & Sani 2000). Indeed, in some cases we observe elemental pressure oscillations of ≈ 2 MPa within the mantle wedge region of our 3-D models. We find that interpolation of the elemental pressures to the nodes removes this pressure mode. In addition, we use the high-resolution, 2-D models to ensure that these artefacts do not exert a significant effect on subduction dynamics: we find that increasing the resolution by a factor of 2 effectively removes this checkerboard effect and, as described above, does not modify the slab dynamics. This gives us confidence in the robustness of our lower resolution, 3-D models.

We take advantage of the system symmetry about the trench-perpendicular axis, which enables us to halve the computational domain in that dimension (Fig. 1). In addition, two of the double slab models (out-dip and in-dip) have an additional plane of symmetry that is parallel to the trenches, allowing yet another halving of the computational domain. In our same-dip configuration (i.e. no additional plane of symmetry), there are 16 777 216 elements which, for our compositional setup, corresponds to 68 145 091 degrees of freedom. For 1500 time steps, such models require ~ 23 hr computation time on 256 CPUs.

3.1 Model, plate and initial slab geometries

We use a model domain size of 7920 km (trench perpendicular) by 5280 km (trench parallel) by 660 km (depth), that is, a model aspect ratio of 12:8:1. We include upper plates for all of the subduction systems, and all plates have trench-parallel widths of 2000 km (Fig. 1). For the single slab reference case, the initial trench-perpendicular length of the subducting plate at the surface is 4000 km, and that of the overriding plate is 2000 km, although we also examine alternative initial plate lengths. For the double slab systems, the initial length of all plates is 2000 km. These dimensions are partially dic-

tated by the domain size because the edges of the model domain need to be far enough from the plates such that they do not exert significant influence on the subduction process (e.g. Stegman *et al.* 2010a).

To prevent unrealistic mantle flow at the surface and large magnitudes of plate shortening in the trench-parallel direction, we include stationary side plates initially separated from the subducting and overriding plates by 25 km of asthenosphere (Fig. 1). Even with a stationary side plate, the 25 km separation typically increases to between 50 and 100 km by the end of the subduction experiment. Models run without side plates yield comparable results in terms of convergence rate and slab dip; the primary difference is more a pronounced shortening of the plates in a trench-parallel direction and, in some cases, subduction initiation at the side of the subducting plate (e.g. Yamato *et al.* 2009).

In order to ensure that our chosen box size is sufficiently large, we test the effect of both wider and longer model domains. For our single slab reference model, increasing the width of the box by a factor of 1.5 results in negligible convergence rate variation (<1.5 per cent), and increasing the box length by a factor of 1.33 results in a convergence rates that is reduced by <4.5 per cent. Because a simple increase in box length should, if anything, act to increase the rate of plate convergence, we believe that the observed slowing of convergence is caused by the increase in length of the side plates, which alters the pattern of flow in the asthenosphere. Similarly, the effect of the box sides on trench motions is minimal. Rather, trench velocities are mainly the result of shear forces acting on the sides of the moving plates by the stationary side plates, as well as shear on the base of the moving plates near the side plate boundaries.

Subduction is initiated by extending the subducting plate below the overriding plate with a centre-line radius of curvature of 150 km. Because the focus of this study is near steady-state behaviour and not subduction initiation, the subducting plate is extended downward to a point near the base of the upper mantle, at $z = 500$ km (Fig. 1). Due to the limitations on plate length imposed by the size of the model domain, this allows for a longer period of near steady-state behaviour than initiating subduction with a shallow slab tip (*cf.* Holt *et al.* 2015). Our definition of near steady-state subduction is that both convergence rate and slab morphology exhibit only minor variations through time, which can be largely attributed to the changing length of the subducting plate at the surface and along the base of the upper mantle.

When subduction is started with an initially shallow slab notch ($z < 150$ km), the slab generally chooses a preferred orientation of subduction atop the model base, that is, a slab that is ‘normally oriented’ (dip angle $\approx 0^\circ$) or ‘overturned’ (dip $\approx 180^\circ$). We will show that when subduction is started with the slab-tip near the base of the upper mantle and the sense of initial dip is in the preferred orientation, the slab rapidly attains a near steady-state geometry and subduction rate. However, when subduction is started with a sense of initial dip that is opposite to the preferred orientation, there is a transition period during which the slab dip inverts to achieve the preferred orientation. This occurs after a period of initial slab bending, the direction of which (i.e. ‘normal’ or ‘overturned’) is dictated by the dip angle imposed near the lower boundary (e.g. Ribe 2010). We examine for which configurations slabs retain their initial sense of dip, or when they adjust to a ‘preferred’ geometry not equivalent to that initially imposed. For normal initiation, we extend the initial portion of the subducting plate to a depth of 500 km with a specified uniform dip of 70° . For overturned initiation, we extend the initial portion of the subducting plate to a depth of 500 km with a specified uniform dip of 95° (Fig. 1).

3.2 Viscosity structure, temperature and composition

To facilitate motion between the subducting and overriding plates, the upper portion of the subducting lithosphere consists of a weak ‘crustal’ layer, 15 km thick, with the same density as the underlying plate and the same viscosity as the asthenosphere. In order to avoid stress discontinuities, the thickness of the low-viscosity crust, defined by compositional tracers, is linearly tapered with depth and replaced by slab lithosphere. At depths ≤ 200 km, the crust has full thickness. For depths ≥ 400 km, the entire crust is replaced by slab lithosphere (see Holt *et al.* 2015, for further details).

We seek a lithospheric viscosity structure such that the bending strength of the plates is not so large as to dominate the evolution of the system (*cf.* Buffet & Becker 2012). Lithosphere–asthenosphere viscosity contrasts of 100–1000 are generally required to produce both the variability in trench-migration regimes inferred to occur on Earth (e.g. Schellart 2004; Fuciniello *et al.* 2008; Becker & Faccenna 2009; Stegman *et al.* 2010b), and are consistent with plate flexure observations (Billen & Gurnis 2005).

Our modeling shows that during double subduction, uniform viscosity plates with a thickness of 80 km and viscosities 500 times that of the asthenosphere, or less, stretch significantly outside of the trench region. This has an effect on subduction velocity as it decouples the rates of trench velocity from the far-field velocity of the overriding plates. (In a non-stretching scenario, the trench velocity and overriding plate velocities are equal.) To stiffen the plates under uniaxial stretching without a large increase in bending stress, we therefore use 80 km thick plates with a viscosity, outside of the ‘crust’, that is 500 times that of the asthenosphere except within a stiff, viscous core that is 20 km thick and centred around the mid-slab (*cf.* Schmeling *et al.* 2008). This configuration is also consistent with standard rheological profiles of the lithosphere that indicate a stronger (viscous plus brittle) lithospheric core sandwiched between a brittle-yielding upper lithosphere and a ductile-yielding lower lithosphere (e.g. Karato & Wu 1993; Buffet & Becker 2012). A stiff core, with a viscosity 10 times larger than the rest of the lithosphere, produces an increase in uniaxial strength of the plates of ~ 4 , with minimal change in the length scale of flexural bending.

3.3 Boundary conditions

From geoid modeling and isostatic rebound studies, it is generally accepted that the viscosity of the lower mantle is at least one order of magnitude greater than that of the upper mantle (e.g. McConnell 1968; Richards & Hager 1984; Mitrovica & Forte 2004). In the interest of simplicity, we assume subduction is completely confined to the upper mantle, and insert an impermeable boundary at the base of the upper mantle (660 km). We choose this option because

it allows for exploration of the roles of local and regional scale flow in the asthenosphere in 3-D and interplate coupling at the trenches, without additional complicating factors.

All sides of the model domain are free-slip, including the lower boundary. We additionally ran each of the subduction configurations with a no-slip basal boundary condition. The main effect of a no-slip basal boundary is a reduction in convergence rates, and a concomitant decrease in mantle flow velocities. For our reference single slab setup ($L_{SP} = 4000$ km), a no-slip base reduces the convergence rate by ≈ 50 per cent. Equivalently, if the asthenosphere viscosity is reduced by 50 per cent in the no-slip case, the convergence and average mantle flow rates are similar between the free-slip and no-slip cases. One persistent difference is that, in single slab systems with a no-slip lower boundary condition, the trenches move more somewhat more rapidly toward the subducting plate relative to the box of the experiment. Nevertheless, we find that the systematics in moving from single to double slab systems is similar for both sets of boundary conditions.

4 RESULTS

4.1 Single slab subduction

We begin with analysis of a reference single slab subduction model, with an initial subducting plate length of 4000 km, before introducing additional slabs. Fig. 2(a) shows the morphological evolution of this single slab and Fig. 3 shows the temporal evolution of the relevant plate kinematics. When subduction is initiated with a 70° dip, it quickly (< 7 Myr) reaches a near steady-state subduction rate of ~ 7 cm yr^{-1} in a normal (i.e. not overturned) orientation (Fig. 3a). At near steady state, slab dip is fairly uniform at 60° – 70° over depths of 150–450 km. The dependence of results on plate length is investigated by varying the initial subducting plate lengths (subducting plate lengths of 2000, 3000 and 4000 km). Results differ only marginally from the reference case, with constant convergence rates of 7–7.5 cm yr^{-1} (Fig. 3a), and dips that are elevated by $\sim 5^\circ$ for a lower subducting plate length of 2000 km (Figs 3b and 4).

4.1.1 Dynamic pressure and slab dip

There are systematic changes in-dip with time that can be related to changes in the dynamic pressure exerted on the slab by the asthenosphere. We define the dynamic pressure difference across the slab, ΔP , as the pressure on the top of the slab minus the pressure on the base of the slab, both sampled in the mid-asthenosphere at a horizontal distance of 30 km from the slab edges. Centred on the mid-asthenosphere ($z = 330$ km), we integrate the pressure over three depths, that is, $\Delta P = 0.25(\Delta P_{210 \text{ km}} + 2\Delta P_{330 \text{ km}} + \Delta P_{450 \text{ km}})$.

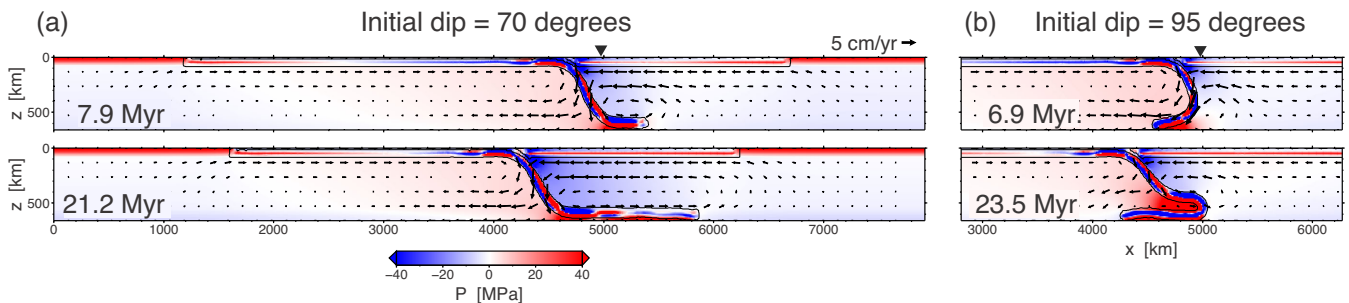


Figure 2. Snapshots of the reference, single slab model with (nodal) dynamic pressure field in colour. (a) Model with an initial slab dip of 70° and (b) model with an initial slab dip of 95° . Overlain are velocity vectors. Inverted triangles indicate the initial trench locations.

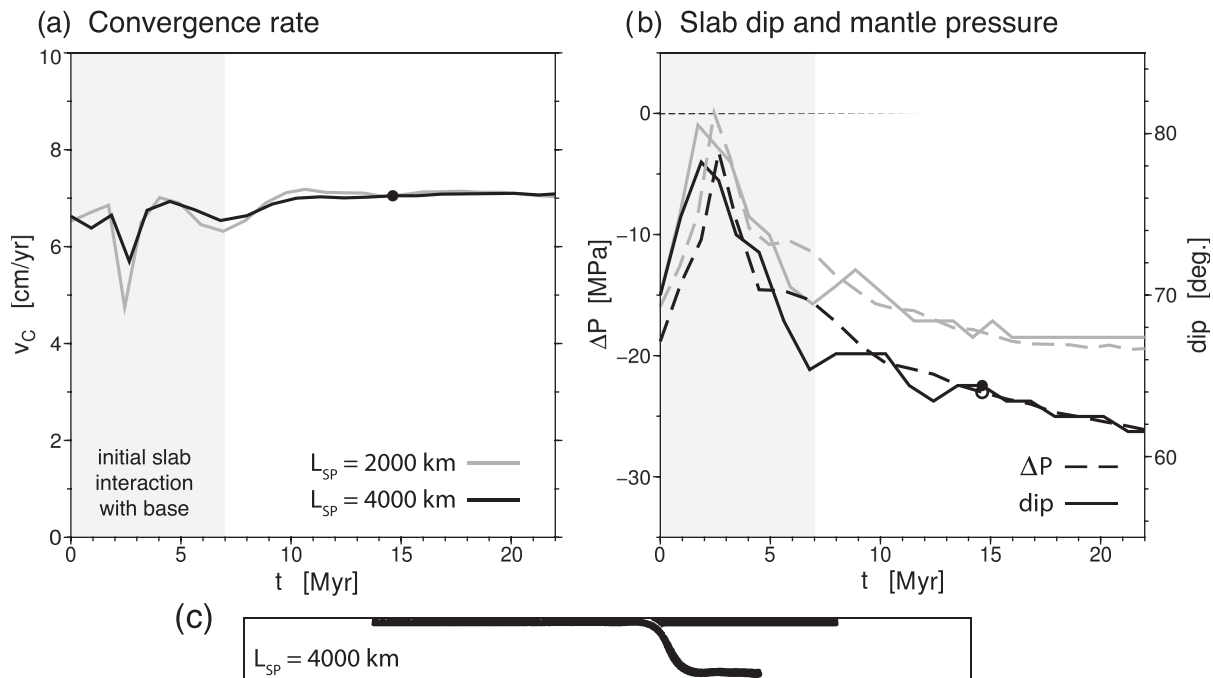


Figure 3. Time evolution of (a) convergence rate and (b) slab dip and dynamic pressure difference (ΔP) across the slab for two single slab models with initial plate lengths of 2000 and 4000 km as described in the text (i.e. Fig. 2a). (c) Slab geometry at time indicated by dots on panels (a) and (b).

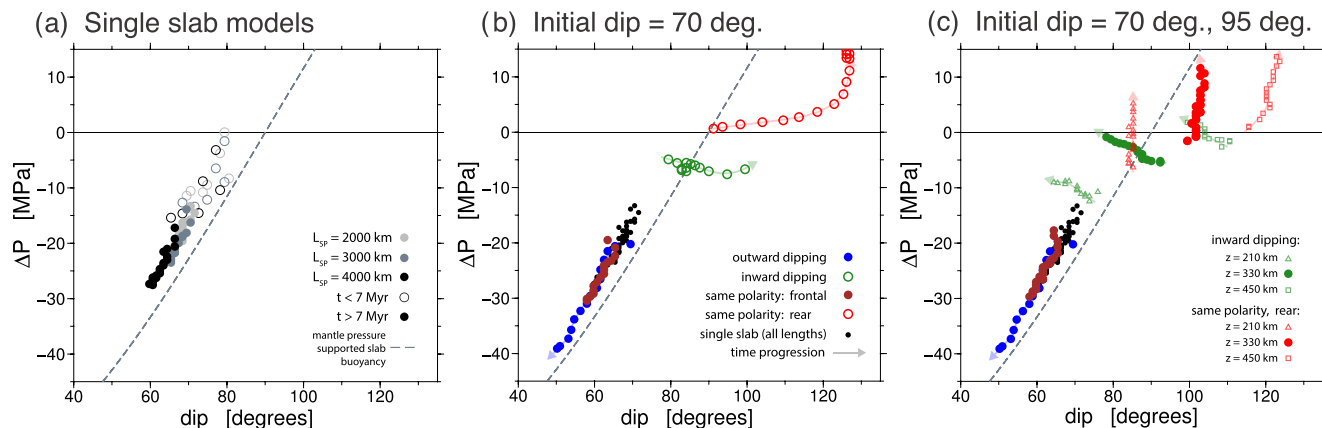


Figure 4. Dynamic pressure differences across slabs (ΔP) plotted versus dip, for single and double subduction systems as indicated. ΔP and slab dip are computed at mid-mantle depth, as described in the text, unless otherwise indicated. Dashed line shows theoretical relationship for slab-normal support of slab buoyancy by pressure on the slab surface (eq. 1). (a) Single slab models with variable plate lengths at early times ($t < 7.0$ Myr, hollow dots) and at near steady-state conditions ($t > 7.0$ Myr, solid dots), (b) double slab models with initial dips of 70° for near steady-state conditions (solid dots), and also models which exhibit non-steady-state behaviour (hollow dots) (all points for $t > 5.5$ – 7.0 Myr, depending on the specific model), (c) double slab models with (same-dip) rear slab subduction initiated at 95° and in-dip slab subduction initiated at 95° (all other slabs initiated at 70°). Arrows on (b) and (c) indicate time progression.

Using our sign convention, a negative ΔP exerts a force directed from the base of the slab toward the top of the slab. (For ease of reference, we designate the top to be the surface that was up when the slab was at the surface, independent of its orientation after subduction into the mantle. This clarification will be needed when we discuss overturned slab geometries.)

In general, ΔP is produced by three, interlinked phenomena. Toroidal flow of asthenosphere around the slab, with dominantly horizontal flow velocities, occurs as the trench and slab move horizontally relative to the side plates. Secondly, the dynamic pressure in the narrowing asthenospheric wedges above and below the slab is affected by corner flow induced by downdip velocity of the slab;

very large pressures can be generated near the narrow tips of the asthenospheric wedges. Lastly, the horizontal motion of the flat-lying slab along the base of the mantle also induces viscous flow that is directed away from the trench in the lower part of the asthenosphere, and toward the trench in the middle part of the asthenosphere. The velocity vectors associated with the latter cases are predominantly in horizontal planes.

In the geometry shown in Fig. 2(a), the portion of the slab that lies flat along the base of the mantle, and which moves to the right relative to the trench, induces counterclockwise flow in the overlying asthenosphere. This counterclockwise flow is associated with a horizontal dynamic pressure gradient within the asthenosphere that

is sandwiched between the flat slab and the overlying plate, with pressure becoming more negative toward the slab. This phenomenon can be broadly understood by considering a simple 2-D equivalent case, where the horizontal flux of the asthenosphere, integrated over a vertical column, must be zero relative to the trench. Because a velocity to the right is imposed on the base of asthenosphere where it is in contact with the flat part of the slab, a horizontal pressure gradient is needed to maintain the zero horizontal flux of asthenosphere. The same general effect occurs in 3-D subduction (although trench-parallel flow becomes more important with increasing distance from the trench).

Similarly, on the other side (left) of the trench, motion of the subducting plate toward the trench induces clockwise flow in the asthenosphere beneath. This clockwise flow is likewise associated with a horizontal dynamic pressure gradient, with pressure becoming more positive toward the slab. However, on the left-hand side (subducting plate side) of the trench, the basal boundary condition on the asthenosphere is free-slip, while on the right-hand side (overriding plate side) it is the velocity set by slab motion above the model base. This means that the magnitude of the horizontal pressure gradient needed to drive flow in the asthenosphere is significantly larger on the right-hand (overriding plate) side of the trench than on the left-hand side of the trench. Thus, the effect of lengthening the flat-lying portion of the slab at the base of the upper mantle dominates the pressure difference across the slab, which becomes progressively more negative with time, varying from approximately -15 MPa at ~ 7 Myr to -26 MPa at 22 Myr (Fig. 3b, black curve).

Figs 3(b) and 4(a) show that slab dip computed at two points centred at 330 km depth (± 80 km) is strongly correlated with ΔP . This is expected from a simple force balance: Wherever slab curvature is near zero and there is little change in slab curvature with distance along a viscous slab, extensional and compressional stresses can be transmitted along the slab, but bending moments within the slab must be small. Therefore, in a region of approximately uniform slab dip, the slab-normal component of gravitational force on the slab should be largely balanced by ΔP . Ignoring bending moments, force balance in a slab-normal direction yields:

$$(\Delta\rho g l) \cos(\theta) + \Delta P = 0 \quad (1)$$

where $\Delta\rho$ is the difference in density between slab and asthenosphere, g is gravitational acceleration, l is slab thickness and θ is slab dip. Note that where $\theta < 90^\circ$, negative ΔP acts to support the slab. Where $\theta > 90^\circ$, positive ΔP acts to support the slab.

For the various plate lengths, pressure and slab dip derived from near steady-state conditions lie near this theoretical relationship with a nearly uniform offset of ~ 5 MPa (Fig. 4a). This indicates that the slab is largely supported, in a slab-normal direction, by dynamic pressure within the asthenosphere. Thus, the dip of the slab is determined by the pressure difference across the slab. Even prior to attaining a near steady-state condition, the single slab cases show a surprisingly good correlation of slab dip to ΔP . We suggest that the reason for the ~ 5 MPa offset in pressure between numerical results and the relation given in eq. (1) is either complications arising from the 15-km-thick weak ‘crust’, or flexural stresses induced by bending at the base of the upper-mantle boundary (see Section 4.2.1 for further explanation).

4.1.2 Preferred orientation for subduction

When we initiate subduction with a short initial slab depth of 150 km, the single slab evolves to the same geometry and con-

vergence rate as the long slab initiated at 70° (Fig. 2a). In order to illustrate the extent to which slabs prefer to subduct in a normal ($\theta < 90^\circ$) or overturned ($\theta > 90^\circ$) geometry, we also initiate single subduction with a long slab at 95° dip (Fig. 2b). Initially, the tip of the subducting plate becomes completely overturned and flattens upside down along the base of the upper mantle. However, the slab does not develop a near steady-state behaviour. Instead, it begins to fold and reverse its direction of dip. It appears that given sufficient time (not reached due to constraints on plate length and model domain size), the slab will attain a normal geometry where it flattens onto the base of the upper mantle at an angle approaching 0° .

Comparing the behaviour of the single slab system initiated in both normal and overturned modes therefore suggests that slabs have a preferred orientation of subduction, which they eventually attain independent of initial dip (*cf.* Di Giuseppe *et al.* 2008; Faccenna *et al.* 2009). This will also be examined for the double subduction systems below, where we show that some slabs have a preference for an overturned geometry (i.e. dip $> 90^\circ$: see Section 5 for further analysis).

4.2 Double slab subduction

Fig. 5 shows the dynamic pressure and velocity fields for three basic, double subduction geometries (Fig. 1). The configurations are: (i) double ‘out-dip’, where the middle plate is subducted along both edges and the plate interfaces dip away from one another; (ii) double ‘same-dip’, where the middle plate and one outer plate are subducted and the plate interfaces dip in the same direction (*cf.* Jagoutz *et al.* 2015); (iii) double ‘in-dip’, where the two outer plates are subducted beneath the middle plate and the plate interfaces dip towards one another. In the Supporting Information, we have also included 3-D movies to illustrate the time evolution of the mantle pressure, and associated mantle flow, for each of the three double slab configurations and the reference, single slab configuration.

4.2.1 Double out-dip subduction

Figs 6 and 7 show the morphological and kinematic evolution of the double out-dip subduction system. Through symmetry, the slabs are mirror images of one another. Dynamic pressures and plate forces are also symmetrical about the mid-line of the middle plate. The evolving geometry of each slab in this double slab system is similar to that of the single slab case. Relative to the single slab case, individual subduction rates are slower by ~ 25 per cent (at ~ 5.5 cm yr $^{-1}$), but the total convergence rate across the entire system is faster than across the single slab system, at ~ 11 cm yr $^{-1}$ (Fig. 7a). Slabs subducting in the double out-dip setting have a strong preference for a ‘normal’ geometry, and, if started in an overturned mode, behave much like the single slab case shown in Fig. 2(b).

The double out-dip and single slab systems both have ‘free’ upper plates; there is no driving force on the plate besides a contribution from a version of ‘ridge push’ at the free ends of the plates. The double out-dip system differs from the single slab case in that the subducting plate does not have free ends. As the middle plate is subducted at both trenches, the trenches and the slabs move towards each other. The concomitant decrease in the volume of asthenosphere between the slabs is accommodated by trench-parallel flow between slabs (Fig. 5a and Supplementary Movie 1). This results in elevated pressure in the asthenosphere between the slabs, which increases as the distance between slabs decreases (e.g. Fig. 6).

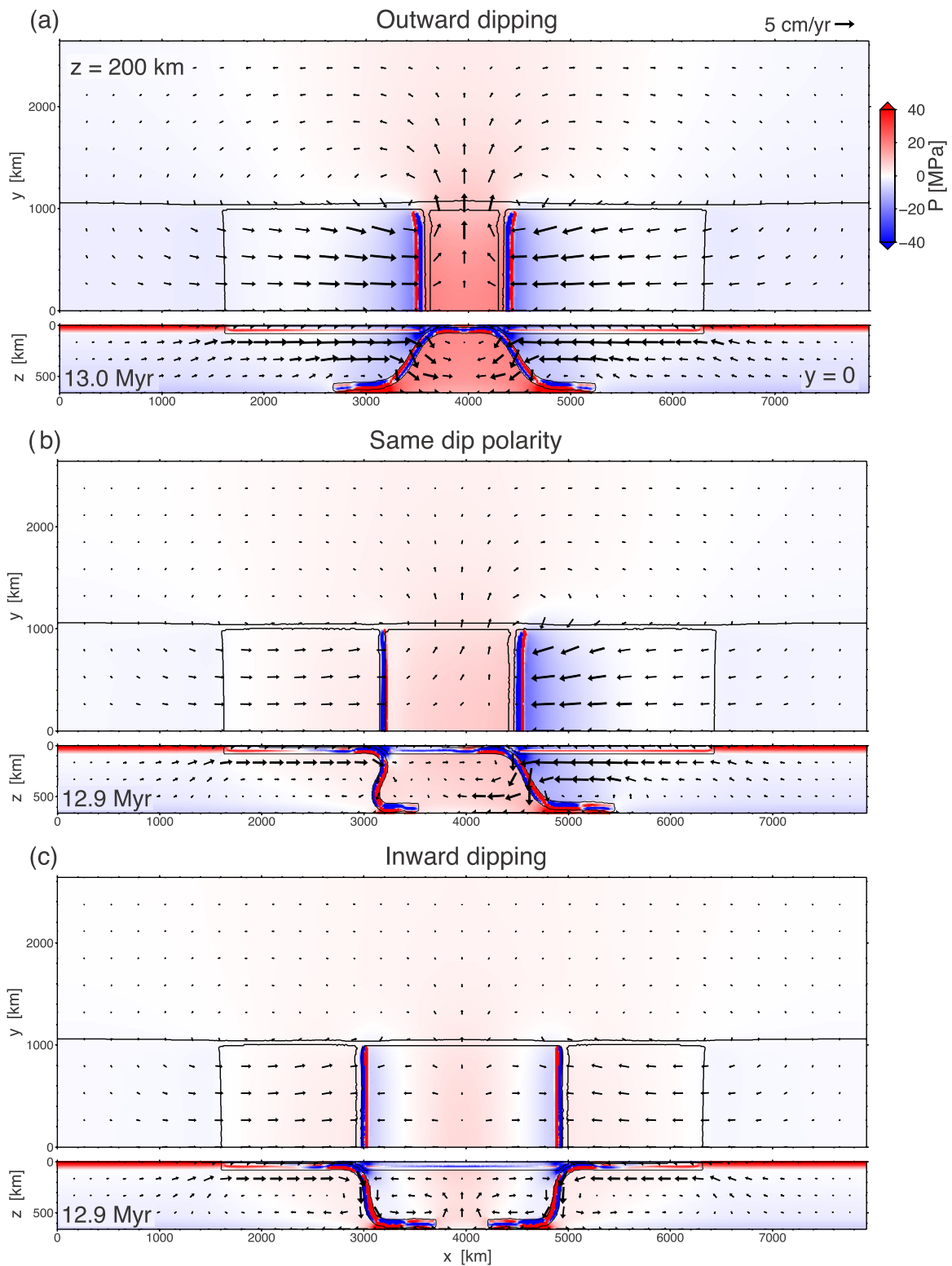


Figure 5. 3-D dynamic pressure (colour) and mantle flow (arrows) fields for double slab subduction models with initial dips of 70° : (a) out-dip, (b) same-dip and (c) in-dip. For each model, the upper panel is a sublithospheric horizontal pressure slice ($z = 200$ km), and the lower panel is a vertical cross-section through the model mid-plane ($y = 0$). For all models, black lines show extent of surface plates in the horizontal slice and subducting slabs in the vertical slice.

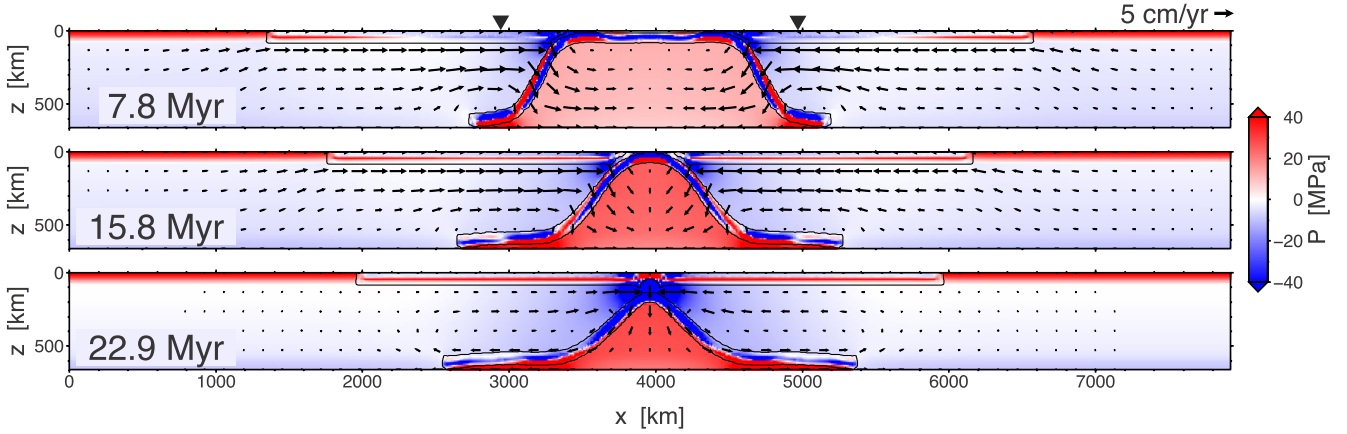


Figure 6. Snapshots showing the model evolution for the out-dip double slab model initiated with a slab dip of 70° with velocity vectors (arrows) and dynamic pressure field (colour). Inverted triangles indicate the initial trench locations.

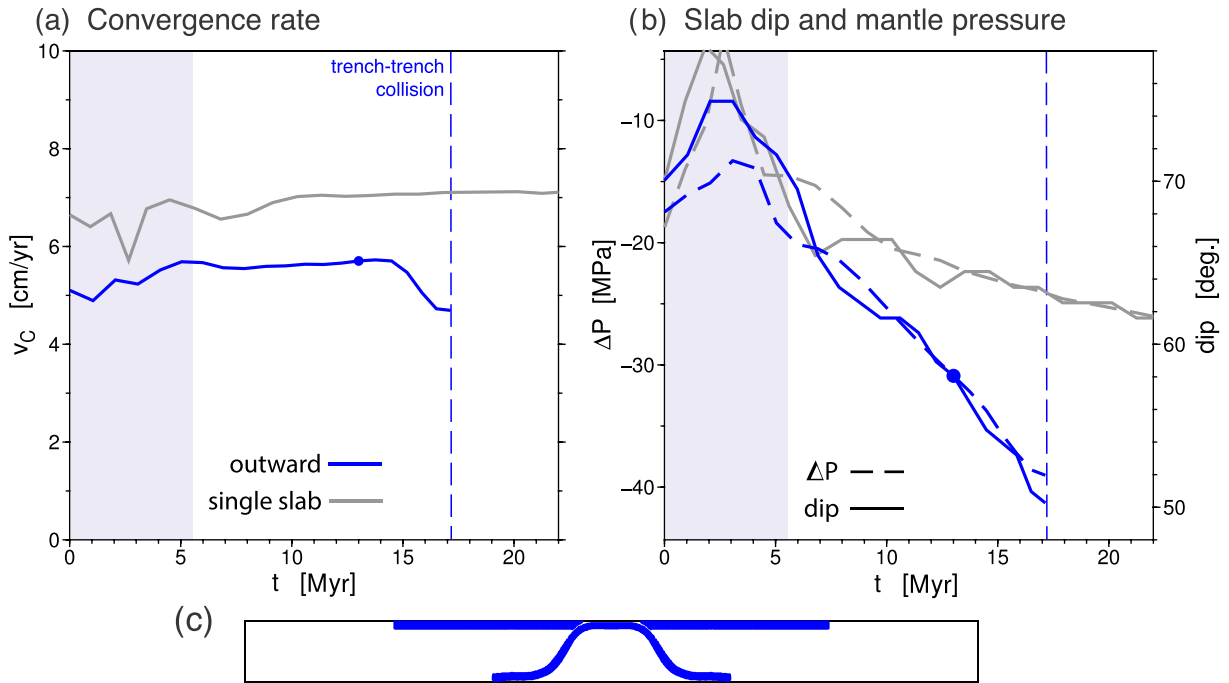


Figure 7. Time evolution of (a) convergence rate, (b) slab dip and dynamic pressure difference (ΔP) across the slab for the out-dip double slab model (Fig. 6) with reference single slab model plotted in dark grey. (c) Slab geometries at times indicated by dots on panels (a) and (b).

As in the case of single slab subduction, slab dip and dynamic pressure, ΔP , correlate through time (Fig. 7b). Points defined by slab dip versus ΔP plot along the trend defined by the theoretical relationship of eq. (1), again with a near-uniform offset of positive ~ 5 MPa (Fig. 4b). This indicates that in double out-dip subduction the slab is supported dominantly, in a slab-normal direction, by the pressure difference across the slab. We suggest that the pressure offset is due to either the low-viscosity ‘crust’, or flexural stresses induced by the support of the lower boundary (which act to reduce the dip angle below that which is supported solely by pressure). For the out-dip case, we ran equivalent models in 2-D, with a deep box (1320 km) and an equivalent depth box (660 km). For the case with equivalent domain height, we found that the 2-D slabs had an equivalent, positive ~ 5 MPa offset, thereby ruling out 3-D effects. For the case with a deep box, ΔP is typically more negative, than in the shallow box models, by 5–10 MPa. For equivalent single slab tests (i.e. 2-D, deep box), ΔP is typically more negative by >10 MPa. We

therefore suggest that the lower boundary does provide additional buoyancy support (i.e. reduces the magnitude of ΔP for a given dip), due to flexural stresses associated with deformation at the lower boundary, but note that the exact magnitude of the pressure offset is not reconciled by these tests.

Relative to the single slab reference, this double slab configuration extends the range of slab dip and dynamic pressure values to shallower dip angles and greater magnitude ΔP (Fig. 4b). The more negative pressure difference across the out-dipping slabs is consistent with their shallower dip as compared to the single slab case. As a function of time, the increase in dynamic pressure beneath the slab and the decrease in slab dip are related to the increasing dynamic pressure between the slabs, and the increase in length of the flat-lying portion of the slab at the base of the upper mantle (Fig. 6).

There are also large extensional forces, up to $\sim 2.5 \times 10^{13} \text{ N m}^{-1}$, transmitted along the middle plate between the two trenches

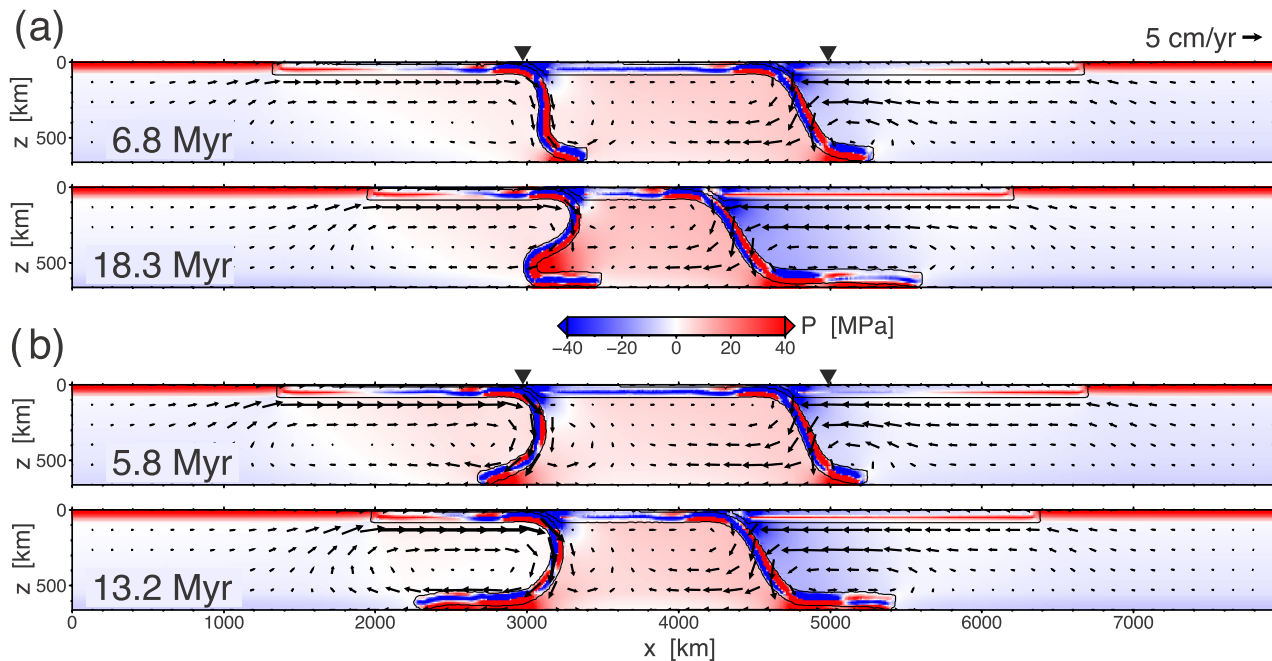


Figure 8. Snapshots showing the model evolution for the same-dip double slab model with velocity vectors (arrows) and dynamic pressure field (colour). For both models, the front (right) slab dip is initially 70° . The initial dip of the rear (left) slab is, (a) 70° and (b) 95° . Inverted triangles indicate the initial trench locations.

(equivalent to an average differential stress through an 80 km plate of ~ 220 MPa). This force may be thought of as slab pull from both subduction systems acting to produce extension within the middle plate (see Section 5.1).

4.2.2 Double same-dip subduction

The same-dip subduction system contains two plate interfaces that dip in the same direction. One slab consists of middle plate lithosphere subducting beneath an outer plate (right plate in Fig. 8), and the other consists of the outer plate lithosphere (left plate in Fig. 8) subducting beneath the middle plate. We will refer to the outward-

dipping (right) slab as the ‘front’ slab and the inward dipping (left) slab as the ‘rear’ slab.

The geometry of the front slab is similar to that of the single slab system. ΔP varies from -17.5 MPa at ~ 7 Myr, to -30 MPa after 20 Myr (Figs 4 and 9c), slightly reduced (i.e. higher magnitude) relative to the single slab reference case. Points corresponding to slab dip versus ΔP for the front slab fall along the theoretical trend predicted by eq. (1), indicating that the slab-normal component of buoyancy is largely supported by the pressure difference across the slab, as in the single and out-dip cases. The front slab exhibits a range of dip and ΔP that are similar to the single slab case, as well as a nearly identical individual convergence rate (Fig. 9a, $v_c \sim 6.5\text{--}7$ cm yr $^{-1}$).

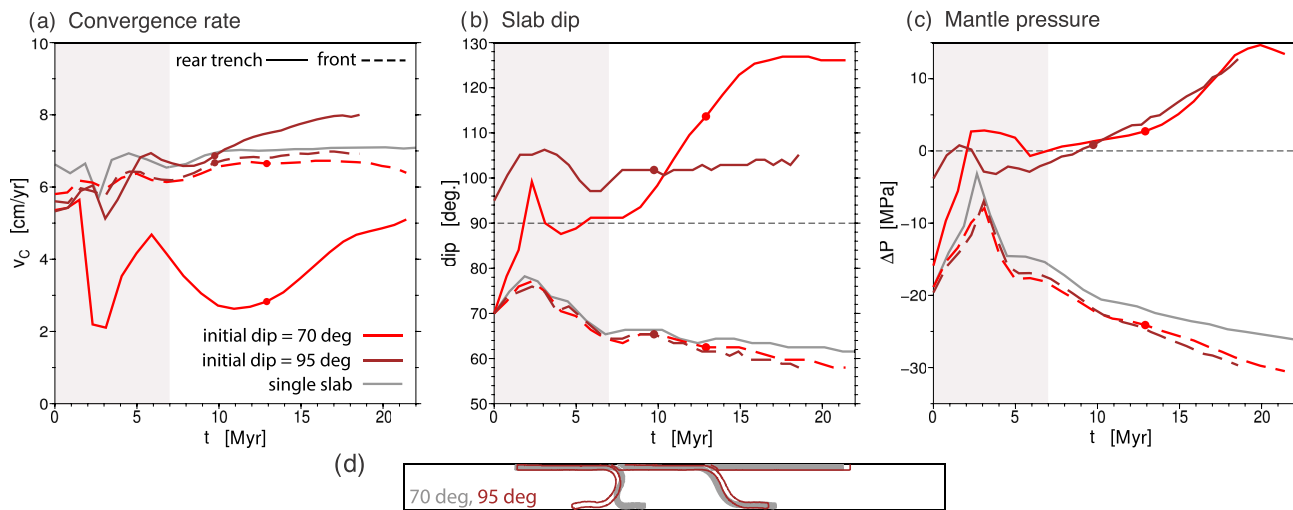


Figure 9. Time evolution of (a) convergence rate, (b) slab dip and (c) dynamic pressure difference (ΔP) across the slab for the same-dip double slab model (Fig. 8) with reference single slab model plotted in dark grey. (d) Slab geometries at times indicated by dots on panels (a)–(c). Results with initial rear slab dip of 70° are in red and results with initial rear slab dip of 95° are in brown.

Like the single slab and double out-dip cases, the front slab exhibits near steady-state behaviour when initiated with a normal slab geometry (i.e. dip = 70°). And, like the single slab and double out-dip cases, when initiated with an overturned slab geometry (not shown), the front slab does not display near steady-state behaviour but rather folds in what appears to be a transition to a normal subduction geometry. Thus, the front slab has a strong preference for subduction in a normal geometry.

The behaviour of the rear slab is very different from that of the front slab (and the single and out-dip slabs). When initiated in a normal geometry, the rear slab does not evolve to near steady-state behaviour. Instead, the slab folds in what appears to be a transition to an overturned geometry (e.g. Supplementary Movie 2). The individual subduction rates are greatly reduced relative to the other models (to between ~ 2.5 and 4 cm yr^{-1}), and are strongly time-dependent throughout duration of the model run (Fig. 9a, red curve)

Folding and overturning of the rear slab can be attributed to the sign of ΔP across the slab. Because higher dynamic pressures are generated between the converging slabs, the rear slab has positive dynamic pressure on its upper surface and lower magnitude, positive dynamic pressure on its lower surface. This results in a positive pressure difference across the front slab, that is, the opposite of that observed for the other slabs. ΔP across the rear slab begins steady-state at near zero and evolves to $\sim 10\text{--}15 \text{ MPa}$ (Figs 4b and 9c). ΔP is more positive than for the front slab by $\sim 17.5 \text{ MPa}$ at 7 Myr, and by $\sim 45 \text{ MPa}$ at the end of the model experiment (Fig. 4b). This positive pressure difference acts to push the rear slab outward (to the left), thereby folding it into an overturned geometry at depth. There is also force acting to pull the rear slab inward (to the right) at the plate interface (i.e. at shallower depth). This may be interpreted as slab pull from the front slab transmitted through the middle plate to the plate interface (see Section 5.1).

The lack of near steady-state convergence rate for the rear slab, and its slow rate of subduction, can be attributed to the folding of the lower slab and strong viscous and flexural support of the slab in the lower asthenosphere (Fig. 8a). Fig. 4(b) shows that during the early phase of subduction, the rear slab has a mid-slab dip that is consistent with slab-normal support by ΔP . However, the pressure–dip relationship soon moves away from that expected for slab-normal support of the slab by dynamic pressure.

Fig. 8(b) shows the geometry of the rear slab when subduction is initiated at 95° . (Note that the frontal slab is still initiated with a dip of 70° .) In this overturned geometry, the rear slab exhibits near steady-state behaviour, maintaining a subduction rate of $\sim 6.5\text{--}8 \text{ cm yr}^{-1}$, similar to the subduction rate for the frontal slab (and the single slab system). This overturned slab shape has a dip that increases from $\sim 45^\circ$ immediately below the overriding plate to nearly vertical at mid-mantle depth and flattens onto the base of the upper mantle with a dip that approaches 180° (Fig. 8b).

In Fig. 4(c), we plot the relationship between ΔP and slab dip for each of the models with their ‘preferred’ initial geometry (i.e. for the same-dip case, the front slab is initiated with a normal geometry, and the rear slab with an overturned geometry). For the rear slab with an overturned geometry, the relationship between ΔP and slab dip computed at mid-asthenospheric depth is shown by red, filled circles. The relationship between ΔP and slab dip begins at early times with a dip that is $\sim 10^\circ$ greater than the 90° dip expected from the near-zero ΔP . As the system evolves, the dip remains approximately constant at 100° , while ΔP increases to $+12 \text{ MPa}$, bringing the relationship close to that ex-

pected for slab-normal support of the slab by viscous stresses in the asthenosphere.

Because a single dip angle is clearly not an adequate representation of the overturned geometry (Fig. 8b), we also show ΔP versus slab dip for deeper (hollow squares) and shallower (hollow triangles) segments of the subducting slab (Fig. 4b). The deeper portion of the slab is more overturned than would be expected from dynamic pressure by, on average, $\sim 20^\circ$. This additional support likely comes from in-slab stresses associated with slab bending as the slab is forced to attain a 180° dip at the base of the upper mantle. The shallow slab segment, in contrast, has a dip angle that is only moderately lower than that expected from pure pressure support, by $\sim 5^\circ$, probably because the dip of the slab as it emerges from beneath the overriding plate is affected by the plate boundary geometry. This indicates that, despite the obvious slab curvature, bending stresses only provide support for the slab in the range of $\sim 10 \text{ MPa}$ in the middle and upper asthenosphere, as compared to the negative slab buoyancy of $\sim 80 \text{ MPa}$. In contrast, support of the overturned slab in the lower asthenosphere can be quite large.

This analysis of same-dip double subduction shows that slabs with a positive ΔP across the mid-slab region have fundamentally different behaviour than slabs with negative ΔP in the mid-slab region. In the former case, slabs prefer to subduct in an overturned geometry and attain near steady-state behaviour only in this configuration. In addition, the overriding plate of the rear slab constitutes the other slab, and so the stress state at the plate boundary is distinct from that of the slabs that have free overriding plates (i.e. all other slabs). The propensity for such slabs to subduct in an overturned geometry is discussed further in Section 5.2.

4.2.3 Double in-dip subduction

Fig. 10 shows how slab geometries evolve when the two outer plates subduct beneath the middle plate (double ‘in-dip’). The double in-dip case is similar to the single slab case in that both subduction systems have ‘free’ subducting plates, with no extension or compression applied at the plate end furthest from the trench (except for ridge push). The double in-dip case is different from the single slab case in that the overriding plate does not have a free end, but is coupled to the downgoing plates on both ends by forces transmitted across the plate contact zone.

We discuss first the case where subduction is initiated at 70° , where near steady-state conditions are not reached (Fig. 10a). Subduction reaches a maximum, individual slab rate of $\sim 6 \text{ cm yr}^{-1}$ after 5 Myr, but after 21 Myr has slowed to $\sim 3.5 \text{ cm yr}^{-1}$. (Fig. 11a). This rate of subduction is slower than that for the double out-dip case, although not as slow as for the rear slab in the same-dip system when initiated with 70° initial slab dip (also not in steady state).

Note that in the latter stages of subduction, as the slab tips approach one another, the dynamics of the system becomes increasingly affected by the force that the slab tips exert on one another through the intervening asthenosphere. This can be seen by the lower panel in Fig. 10(a), where large, positive dynamic pressures have developed between the slab tips by $\sim 17 \text{ Myr}$, and a transient mantle upwelling is localized above the void between the two slab tips. However, the region of positive dynamic pressure is sufficiently localized in the lowermost asthenosphere that it has little effect on pressure in the upper asthenosphere or the forces transmitted through the overlying plate (see Section 5.1). Once the

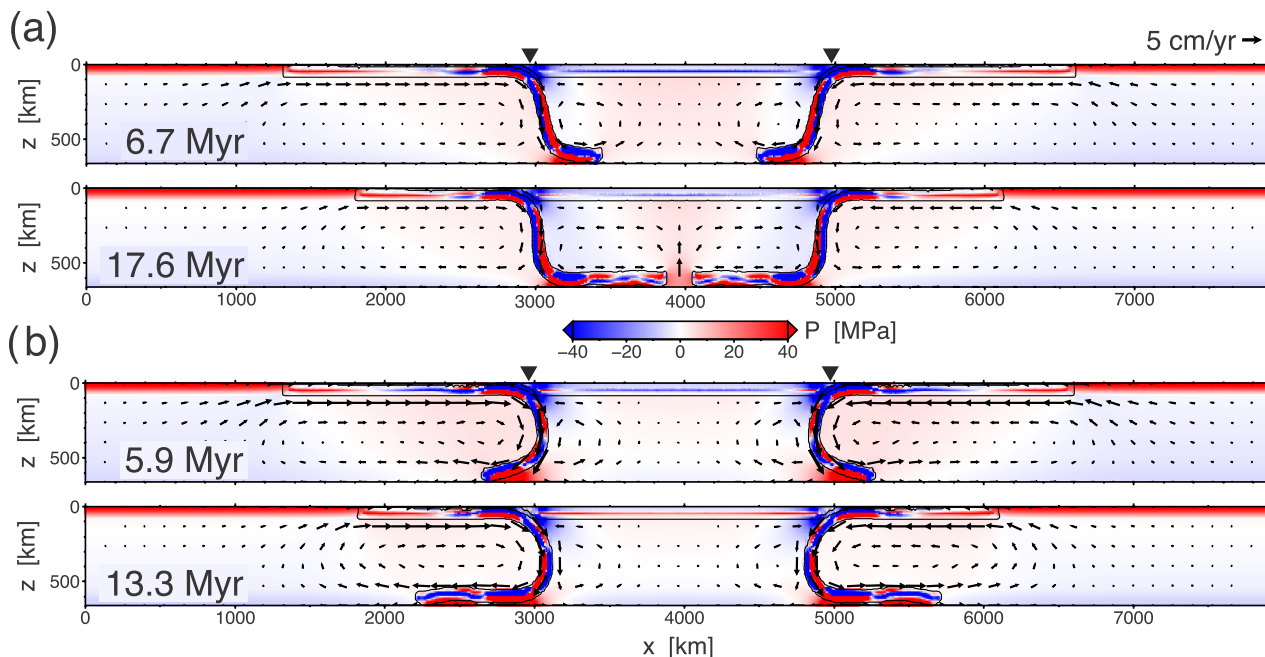


Figure 10. Snapshots showing the model evolution for the in-dip double slab model with velocity vectors (arrows) and dynamic pressure field (colour). The initial dip of the slabs is (a) 70° and (b) 95° . Inverted triangles indicate the initial trench locations.

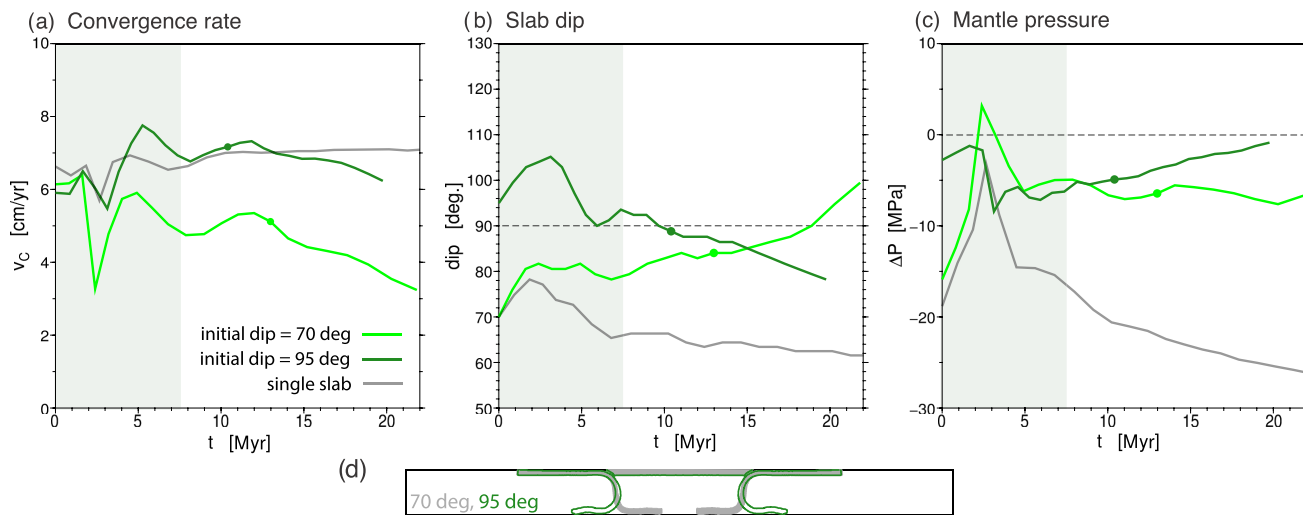


Figure 11. Time evolution of (a) convergence rate, (b) slab dip and (c) dynamic pressure difference (ΔP) across the slab for the in-dip double slab models (Fig. 10) with reference single slab model plotted in dark grey. (d) Slab geometries at times indicated by dots on panels (a)–(c). Results with initial slab dip of 70° are in light green and results with initial slab dip of 95° are in dark green.

slab tips become sufficiently close, the subduction system effectively shuts down, with rapidly decreasing plate convergence rates. While interesting, this is not a part of the subduction process that we wish to analyse in this paper and we focus instead on the slab evolution prior to this time.

Despite the lack of near steady-state subduction, ΔP versus slab dip plots on the line predicted by eq. (1) (Fig. 4b), particularly during the earlier subduction phase (i.e. prior to significant pressure build up between the two slab tips). Slab dip at mid-mantle depth is approximately 80° after steady-state subduction is established (i.e. after initial slab interaction with the lower boundary: $t > 7.5$ Myr)

and increases to 90° at ~ 19 Myr (Fig. 11b). The ΔP across the mid-slab is approximately constant at -6 MPa, significantly less negative than ΔP in the single slab system.

The failure to attain a near steady-state subduction rate suggests that in-dipping slabs have a preference for subduction in an overturned geometry (Fig. 10b). When subduction is initiated at 95° , the system attains near steady-state behaviour after ~ 7.5 Myr, although subduction rates decrease slightly from ~ 7.3 to ~ 6.3 cm yr^{-1} . The overturned slab geometry is similar to that of the rear slab in the same-dip configuration (*cf.* Figs 8b and 10b). The near steady-state individual subduction rate is similar to that of the single slab

reference case, the frontal slab in the same-dip geometry, and the rear slab in the same-dip geometry when subducting in an overturned geometry. Therefore, aside from the outward dipping slabs, slabs that are initiated in their preferred geometry attain individual slab convergence rates very close to that of the single slab reference.

Plotted on Fig. 4(c) is ΔP versus slab dip for in-dip subduction initiated in the overturned geometry. At mid-mantle depth, where the slab is near vertical, values of ΔP versus slab dip fall near or on the theoretical relationship of eq. (1). However, within the upper and lower asthenosphere, flexural stresses can be quite large and play a greater role in dictating slab dip.

5 DISCUSSION

5.1 Intraplate stress, plate coupling and dynamic pressure

Examination of the pressure and stresses within the asthenosphere shows that, except near the slabs and beneath the boundaries with the side plates, viscous flow in the asthenosphere is almost entirely driven by horizontal pressure gradients. Near the slab surfaces, slab-normal deviatoric stresses in the asthenosphere are negligible (less than ~ 0.5 MPa) compared to dynamic pressure, which is typically in the range of tens of megapascals. Thus, the viscous forces applied to the slabs and plates by the asthenosphere are effectively equal to the dynamic pressure. (Here, we will use the term ‘plate’ to mean the unsubducted portion of the plate, not including the slab.) In contrast, within the plates and slabs, deviatoric stresses are commonly large and dominate deformation. For the purposes of the force balances presented below, full stress components must therefore be used within the plates while dynamic pressure can be used in the asthenosphere.

Fig. 12(a) illustrates how dynamic pressure in the asthenosphere and the horizontal forces transmitted through the plates are related. In this simplified 2-D example, the dynamic pressure in the asthenosphere is taken to be zero along the left-hand side of the box.

Therefore, on the right-hand side of the box, the vertically integrated pressure within the asthenosphere ($P_o \times d$) must be balanced by the horizontal force, F , acting on the plate. The latter can be transmitted to another plate, or slab, across a subduction interface as a ‘plate coupling’ force, and so is directly related to interplate forces at the plate contact zone.

Fig. 12(b) shows a comparison between the horizontal, vertically integrated, trench-perpendicular stress (or force per unit length) within the middle plate measured mid-way between the trenches, and the same force estimated by the simple force balance illustrated in Fig. 12(a). (In this case, the integrated pressure at the edge of the box is not necessarily zero, but is always small. ‘Ridge push’, which is $\sim 2.7 \times 10^{12}$ N m $^{-1}$ for the parameters used in this paper, is automatically included.) The points plot on a linear trend with a slope of unity, and close to the theoretical prediction from a simple 2-D force balance.

The difference between the observed and predicted values comes largely from shear stresses on the vertical boundaries between the moving plates and the stationary side plates, as well as shear stresses on the base of the moving plates in a narrow zone near the side plates. We estimate the force provided by these effects to total $\sim 2 \pm 1 \times 10^{12}$ N m $^{-1}$ for plates moving at 7 cm yr $^{-1}$. (The total force exerted by shear on the sides of the moving plates is estimated by observing that the gap between the moving and side plates typically widens to 35–100 km, depending on the experiment. Assuming a velocity difference of 7 cm yr $^{-1}$ multiplied by a viscosity of 2.8×10^{20} Pa s and divided by a shear zone width of 50 km yields a side plate stress of ~ 12 MPa. This can be multiplied by the area of the side of the plate, $\sim 1000 \times 80$ km 2 , divided by the trench-parallel plate width, 2000 km, and doubled to account for both sides of the plate, to yield an estimated force per unit length of $\sim 1 \times 10^{12}$ N m $^{-1}$. There is also shear on the base of the moving plate near its side boundary, which we estimate approximately doubles this figure to $\sim 2 \times 10^{12}$ N m $^{-1}$, with the estimated uncertainty of $\pm 1 \times 10^{12}$ N m $^{-1}$ being due to variation in side gap width and length of the moving plate.)

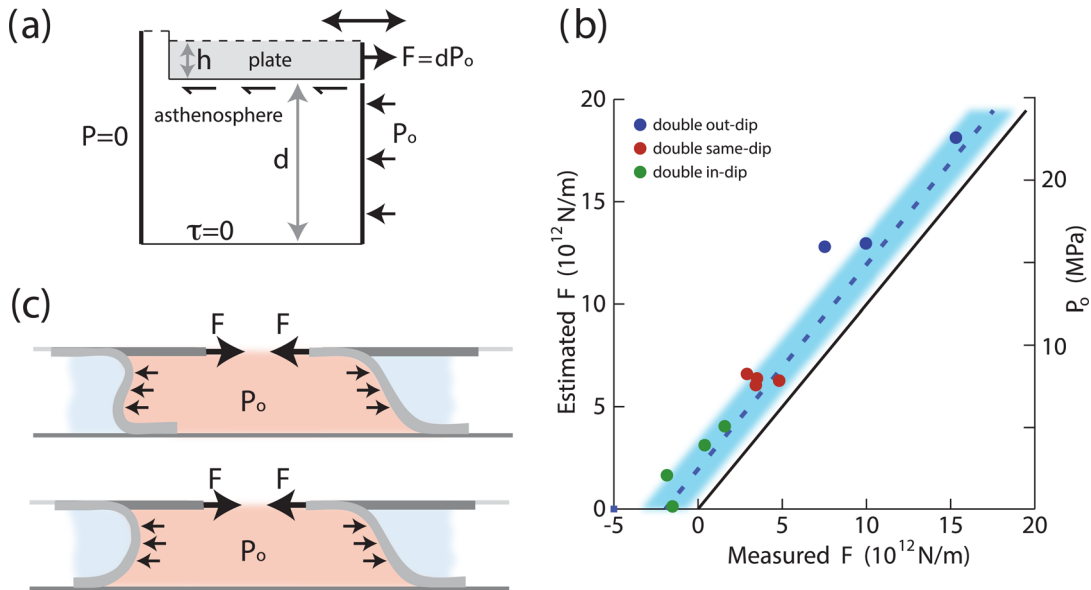


Figure 12. (a) Sketch showing how average dynamic pressure in the asthenosphere (P_o) is related to intraplate force (F) for a simple 2-D example with zero pressure in the asthenosphere on the left-hand side of the sketch. (b) For double slab models, directly measured intraplate force (F) plotted against intraplate force (left vertical axis) computed from averaged asthenospheric pressure P_o (right vertical axis) as per panel (a). Solid line shows one-to-one relationship; dotted line and shaded blue area shows estimate of correction for shear forces transmitted from the side plates. (c) Sketch showing connection between asthenospheric pressure beneath middle plate and intraplate force within the middle plate as applied to the double slab, same-dip plate configuration where the rear slab is initiated in a normal (top) or overturned (bottom) geometry.

This line of reasoning, and the correlation shown in Fig. 12(b), demonstrates a direct correspondence between the dynamic pressure in the asthenosphere and the stress transmitted through the middle plate for our 3-D models, and provides a powerful tool for understanding the differing behaviours of such subduction systems.

Consider, for example, the same-dip case, reproduced in cartoon form in Fig. 12(c). Subduction of the middle plate requires the two slabs to become closer to one another, resulting in positive dynamic pressure within the asthenosphere between the slabs. The force-balance concept shows that the large positive pressure in the asthenosphere must be accompanied by horizontal force (trench normal) transmitted through the middle plate. If one were to cut the middle plate as shown in Fig. 12(c), the horizontal force on this plate end would approximately counterbalance the vertically integrated pressure in the underlying asthenosphere. This means that the middle plate must be in extension, and that the magnitude of the extensional force is approximately equal to the vertically integrated pressure in the underlying asthenosphere.

The same process, that is, positive dynamic pressure in-between the slabs exerting a wedge-directed force, keeps the front (right) slab and both slabs in the double out-dipping configurations stable in a normal configuration and unstable in an overturned configuration (Fig. 6). The opposite is true for the rear slab (left) in the same-dip configuration. The double in-dipping configuration is effectively neutral because the trenches do not converge in this geometry. The small difference in dynamic pressure across the slabs, and correspondingly small force within the mid-plate and transmitted to the plate interface, is not large enough to change the from a normal slab geometry to overturned, and *vice versa*.

The approximate force balance illustrated in Fig. 12(c) works particularly well because the lower boundary of the model is free-slip, and thus exerts no shear stress on the base of the asthenosphere. However, a similar force balance is possible for subduction systems with different boundary conditions at the base, provided that the effects of shear on the base of the upper mantle are accounted for. The preference for slabs to subduct in a normal or overturned geometry is therefore a product of stress transmitted through the middle plate to the plate interface, and of the viscous stress of the asthenosphere acting on the surfaces of the slabs. In fact, these perspectives are nearly identical as they are closely linked within same dynamic system (e.g. Fig. 12).

Note that without a lithospheric rheology that sufficiently resists stretching (e.g. plates with viscoplastic yielding), the stretching of the middle plate will result in a reduction in extensional stress and a concomitant reduction in the dynamic pressure within the underlying asthenosphere. Thus, a rheology that allows significant stretching of the middle plate will change the dynamics of the subduction process by reducing both the extensional force transmitted to the trench, and the pressure difference across the subducting slab.

Using the dynamic pressure within the crustal channel as a proxy for plate coupling force, we can compare the coupling in the various subduction systems. Fig. 13 shows the temporal evolution of the average crustal pressure at mid-lithospheric depths ($z = 40$ km). Except for the rear slab in the same-dip system, all plate coupling interfaces show dynamic pressures that are comparable and become more positive with time, with a total change of +60–80 MPa from the onset of near steady-state behaviour until the end of the experiments. This can be directly linked to the increase in length of the subducting slab along the base of the upper mantle.

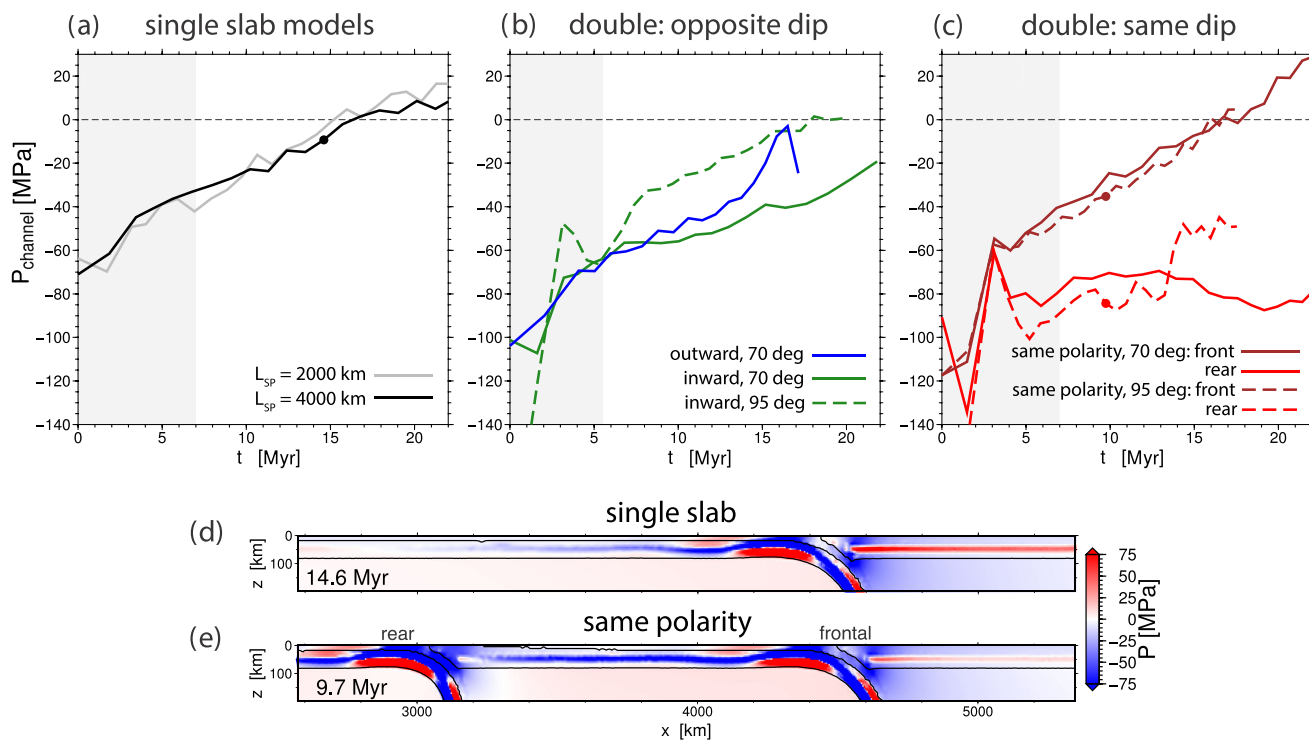


Figure 13. Plate coupling force as function of time, using the average dynamic pressure in the weak crustal channel (at 40 km depth) as a proxy. (a) Single slab models, (b) double slab in-dip and out-dip and (c) double slab same-dip models. The lower panels show dynamic pressure zoomed into the trench regions for, (d) the long subducting plate single slab model, and (e) the same-dip model (initial rear slab dip = 95°). The extracted, average channel pressure for these time steps (d) and (e) is shown by points on panels (a) and (c).

In contrast to the other slabs, the rear slab in the same-dip subduction system exhibits a plate coupling force that remains low (less positive), at about -80 MPa, throughout the experiment. This can be linked to the extensional forces induced in its overriding (middle) plate throughout the evolution of the subduction system and, in turn, the positive dynamic difference across the rear slab (e.g. Fig. 12c). Unlike all the other slabs in this study, where extensional forces are mainly confined to the subducting plate and can be transmitted to the slab without crossing the plate interface, the extensional forces generated in the overriding plate of the rear slab are transmitted across the plate coupling interface from the frontal, subducting plate.

5.2 Trench motion and ‘preferred’ slab geometry

Because the lower boundary of the model is free-slip, the side plates provide the only stationary frame of reference for the subduction system. The coupling mechanism to the reference frame in this set-up is different than in the case of a no-slip lower boundary and absolute trench motions cannot be exactly compared under the two different types of boundary conditions. With this caveat, we can describe the motion of the trenches as advancing or retreating in the reference frame of the side plates and, most robustly, as advancing or retreating relative to the other trench in the system.

By ‘advancing’ we mean that the down-dip direction of the plate interface and the direction of motion of the trench, are the same. By ‘retreating’, we mean the opposite. With this terminology, both trenches in the double in-dip geometry are approximately stationary (Fig. 10). The rear (left) trench is advancing in the double same-dip subduction system (Fig. 8). All other trenches, including single slab subduction, are retreating, which is the common mode in typical numerical modeling studies, and seems to be preferred in nature (e.g. Funicicello *et al.* 2008; Becker *et al.* 2015). In the examples shown here, these designations are the same for absolute and relative trench motions.

When viewed from this perspective, all retreating slab geometries display a strongly negative difference in dynamic pressure, ΔP , applied to the mid-slab from the asthenosphere (Fig. 4), and thus a lithospheric, plate coupling force directed towards the subducting plate (i.e. in the retreat direction; Fig. 12). These slabs also have a strong preference for normal geometry subduction and, if initiated with an overturned geometry, fold as they begin to acquire a normal geometry. The one advancing slab displays positive ΔP , has an overriding plate-directed coupling force (i.e. in the advance direction), and has a strong preference for subduction in an overturned geometry. The stationary, inward-dipping slabs exhibit weakly negative ΔP and show stable subduction geometries in either configuration (although they exhibit faster, near steady-state subduction velocities only in the overturned position).

This simple analysis shows that the inherent preference of slabs to advance or retreat, and to subduct in a normal or overturned geometry, is modified by the presence of another slab in the system. This is attributable both to changes in the dynamic pressure on the slab within the asthenosphere, and the associated changes in coupling forces at the plate interface. Thus, the preferred sense of subduction, and trench migration, is directly related to the orientation of the trenches within a multi-slab system.

5.3 Natural examples

Although natural examples of double subduction with closely spaced slabs may be rare, at least two can be identified in

recent geological time. The Philippine Sea plate is an active example of double subduction in a same-dipping geometry. Simplified 2-D subduction geometries (equivalent to infinite trench width) have recently been used to propose slab–slab interactions as the driver for trench advance in some portions of the Pacific–Philippine Sea plate boundary (Čížková & Bina 2015).

The Philippine Sea system is a 3-D setting, with roughly equal trench lengths and distance between slabs. It differs in some important ways from the same-dip system described here in that the two subduction systems merge to the north where the ‘outside’ plates (Eurasia and Pacific) are juxtaposed across a single subduction boundary, and the ‘middle’ plate (Philippine) is much younger and more extended than the other two plates. Hence, the assumed uniform lithospheric structure for all three plates, and the rectangular plate geometry used here is not directly applicable to that system. Despite this, our 3-D same-dip models with finite width trenches generate the observed retreating motion of the front slab (Philippine), and advancing motion of the rear, Pacific slab (e.g. Čížková & Bina 2015). Additionally, these models exhibit trench-parallel flow in the asthenosphere between the two slabs, in broad agreement with Anglin & Fouch’s (2005) interpretation of shear wave splitting measurements beneath the Philippine Sea plate, and trench perpendicular extensional force within the middle plate, consistent with observed spreading orientation in the backarc region of the Pacific subduction zone. However, additional work which takes into account more complex lithospheric rheologies (to facilitate backarc spreading) and non-parallel trench orientations, is required to directly apply the modeling results to this region.

A second natural example of double subduction has been identified in the northern Tethys region where same-dip subduction occurred over at least 70 Myr, and probably much longer (Jagoutz *et al.* 2015). This culminated in the collisions of Arabia and Eurasia with an intra-oceanic arc system from 90 to 80 Ma, followed by final collisions of India and Arabia with Eurasia after 40 Ma. Between approximately 80 and 50 Ma, same-dip double subduction occurred between India and Eurasia with an approximately rectangular middle plate with a trench-parallel width of approximately 3000 km. Thus, this natural example has a geometry similar to that modeled in this paper. Both the natural example and model results show a total rate of convergence that is approximately twice that of single slab subduction, explaining the ultra-fast convergence of India and Eurasia from 80 to 50 Ma, at ~ 15 cm yr⁻¹ as compared to the maximum single slab rates observed at 7–8 cm yr⁻¹. From a purely kinematic perspective, the intra-oceanic trench was also advancing towards the Eurasian subduction system, a feature consistent with the modeling results.

Our modeling suggests that elevated total plate convergence is a feature not only associated with same-dip double subduction, but is a feature of all double slab rectangular configurations, irrespective of the relative dip polarities. Given the apparent ubiquity of double subduction in many plate tectonic reconstructions, double subduction may therefore provide an appealing way to reconcile plate kinematics that do not fit within the framework of single slab subduction.

6 CONCLUSIONS

This study not only illuminates the dynamic processes that control multi-slab systems, but also sheds light on the dynamics of subduction in general because it extends the range of dynamic

pressures and forces under which subduction occurs. Dynamic pressure differences across slabs in near steady-state subduction are clearly correlated with slab dip. In particular, the net slab-normal viscous stress on slabs that are not completely overturned at the base of the mantle correlates near-linearly with the slab-normal component of slab (negative) buoyancy. (For reference, the buoyancy force associated with the slab correlates with a pressure of ~ 80 MPa for a horizontal slab.) This relationship holds over at least a 50° range of dip (from 50° to 100°) and a 50 MPa range in ΔP (from -40 to 10 MPa), over which there is a uniform discrepancy of approximately 5 MPa.

Double subduction systems can be understood using the same physical concepts as single slab systems. Slab dip is set mainly by net, dynamic pressure on the slab, ΔP . The mid-plate and plate-coupling stresses can be approximately computed by a force balance that equates the net force applied to the slab by dynamic pressure in the asthenosphere with an equal and opposite force applied at the plate interface or within the middle plate (e.g. Fig. 12). The difference in behaviour of the single and double subduction systems is thus attributable to the difference in trench geometry and dip direction, which gives rise to different values of ΔP acting on the slabs, and hence to different magnitudes of plate coupling force and mid-plate stresses.

The combined effects of dynamic pressure and plate-coupling forces exert a net torque on the plate about a trench-parallel axis. This leads to stable subduction in a geometry where the other forces in the system (such as slab buoyancy) counterbalance that torque. The sense of the torque applied by the dynamic pressure and plate-coupling forces induce differences in slab dip and the sense of overturning observed in the various subduction systems. Similarly, the advancing or retreating sense of each trench, relative to the other trench in the system, is also strongly correlated with the force transmitted through the middle plate to the plate interface at the trench, and the pressure difference applied to the slab in the asthenosphere.

All retreating trench systems exhibit plate-coupling forces directed away from the overriding plate between 7×10^{12} and 2×10^{13} N m $^{-1}$ and strongly negative values of ΔP , typically between -20 and -40 MPa; these also lead to stable subduction in a 'normal' geometry (i.e. dip angle $< 90^\circ$). The one advancing slab (rear slab in the same-dip subduction geometry) exhibits a plate coupling force directed toward the overriding plate with a magnitude of $\sim 7 \times 10^{12}$ N m $^{-1}$, positive values of $\Delta P \leq 10$ MPa and stable subduction in an overturned geometry (dip $> 90^\circ$). It is also the only subduction system whose overriding plate is subducting (left plate, Fig. 5c). In the in-dip model, the small magnitude of both ΔP (-7 to 0 MPa) and the plate coupling force results in near-stationary trenches, which are stable in either a normal or overturned configuration.

Transmission of force through the middle plate is critical in controlling the slab geometry and the advancing or retreating sense of the trenches. This study of double subduction systems highlights the importance of the overriding plate (e.g. Yamato *et al.* 2009) because, except in the double out-dip case, the middle plate forms the upper plate to at least one of the subduction zones in the system. The inclusion of an upper plate is not only crucial for the transmission of stress within the plates but, as demonstrated in this paper, is crucial for the development of large magnitude dynamic pressure between the slabs. Hence, the dynamic pressure that acts on, and partially controls, the behaviour of the subducting slabs are linked to the presence, and rheological properties, of the middle plate.

ACKNOWLEDGEMENTS

We thank Claudio Faccenna for insightful discussions about double subduction dynamics in the Western Pacific, and Cedric Thieulot and one anonymous reviewer for comments which significantly improved the manuscript. We also thank the original authors and CIG (geodynamics.org) for providing CitcomCU. The modified code version used in this study is available upon request to the authors. Computation for the work described in this paper was supported by the University of Southern California's Center for High-Performance Computing (hpc.usc.edu), and most figures were made using the Generic Mapping Tools (Wessel *et al.* 2013). AFH and TWB were partially supported by NSFEAR- 1460479 and EAR- 1215720.

REFERENCES

- Anglin, D.K. & Fouch, M.J., 2005. Seismic anisotropy in the Izu-Bonin subduction system, *Geophys. Res. Lett.*, **32**, L09307, doi:10.1029/2005GL022714.
- Becker, T.W. & Faccenna, C., 2009. A review of the role of subduction dynamics for regional and global plate motions, in *Subduction Zone Geodynamics*, pp. 3–34, eds Lallemand, S. & Funicello, F., Springer.
- Becker, T.W., Faccenna, C., O'Connell, R.J. & Giardini, D., 1999. The development of slabs in the upper mantle: insights from experimental and laboratory experiments, *J. geophys. Res.*, **104**, 15 207–15 226.
- Becker, T.W., Schaeffer, A.J., Lebedev, S. & Conrad, C.P., 2015. Toward a generalized plate motion reference frame, *Geophys. Res. Lett.*, **42**, 3188–3196.
- Bellahsen, N., Faccenna, C. & Funicello, F., 2005. Dynamics of subduction and plate motion in laboratory experiments: insights into the "plate tectonics" behavior of the Earth, *J. geophys. Res.*, **110**, B01401, doi:10.1029/2004JB002999.
- Billen, M.I., 2009. Modeling the dynamics of subducting slabs, *Ann. Rev. Earth Planet Sci.*, **36**, 325–356.
- Billen, M.I. & Gurnis, M., 2005. Constraints on subducting plate strength within the Kermadec trench, *J. geophys. Res.*, **110**, doi:10.1029/2004JB003308.
- Buffet, B. & Becker, T.W., 2012. Bending stress and dissipation in subducted lithosphere, *J. geophys. Res.*, **117**, B05413, doi:10.1029/2012JB009205.
- Carlson, R.L. & Melia, P.J., 1984. Subduction hinge migration, *Tectonophysics*, **102**, 399–411.
- Čížková, H. & Bina, C., 2015. Geodynamics of trench advance: insights from a philippine-sea-style geometry, *Earth planet. Sci. Lett.*, **430**, 408–415.
- Conrad, C.P. & Hager, B.H., 1999. Effects of plate bending and fault strength at subduction zones on plate dynamics, *J. geophys. Res.*, **104**, 17 551–17 571.
- Di Giuseppe, E., van Hunen, J., Funicello, F., Faccenna, C. & Giardini, D., 2008. Slab stiffness control of trench motion: insights from numerical models, *Geochem. Geophys. Geosyst.*, **9**, Q02014, doi:10.1029/2007GC001776.
- DiLeo, J.F., Walker, A.M., Li, Z.-H., Wookey, J., Ribe, N.M., Kendall, J.-M. & Tommasi, A., 2014. Development of texture and seismic anisotropy during the onset of subduction, *Geochem. Geophys. Geosyst.*, **15**, doi:10.1002/2013GC005032.
- Duarte, J.C., Schellart, W.P. & Cruden, A.R., 2013. Three-dimensional dynamic laboratory models of subduction with an overriding plate and variable interplate rheology, *Geophys. J. Int.*, **195**, 47–66.
- England, P. & Wilkins, C., 2004. A simple analytical approximation to the temperature structure in subduction zones, *Geophys. J. Int.*, **159**, 1138–1154.
- Enns, A., Becker, T.W. & Schmeling, H., 2005. The dynamics of subduction and trench migration for viscosity stratification, *Geophys. J. Int.*, **160**, 761–775.
- Faccenna, C., Di Giuseppe, E., Funicello, F., Lallemand, S. & van Hunen, J., 2009. Control of seafloor aging on the migration of the Izu-Bonin-Mariana trench, *Earth planet. Sci. Lett.*, **288**, 386–398.

- Funiciello, F., Faccenna, C., Giardini, D. & Regenauer-Lieb, K., 2003. Dynamics of retreating slabs: 2. Insights from three-dimensional laboratory experiments, *J. geophys. Res.*, **108**, doi:10.1029/2001JB000896.
- Funiciello, F., Faccenna, C., Heuret, A., Lallemand, S., Di Giuseppe, E. & Becker, T.W., 2008. Trench migration, net rotation and slab-mantle coupling, *Earth planet. Sci. Lett.*, **271**, 233–240.
- Funiciello, F., Moroni, M., Piromallo, C., Faccenna, C., Cenedese, A. & Bui, H.A., 2006. Mapping mantle flow during retreating subduction: laboratory models analyzed by feature tracking, *J. geophys. Res.*, **111**, doi:10.1029/2005JB003792.
- Gresho, P.M. & Sani, R.L., 2000. *Incompressible Flow and the Finite Element Method*, Volume 1: *Advection-Diffusion and Isothermal Laminar Flow*, John Wiley and Sons, Inc.
- Holt, A.F., Becker, T.W. & Buffett, B.A., 2015. Trench migration and overriding plate stress in dynamic subduction models, *Geophys. J. Int.*, **201**, 172–192.
- Holt, A.F. & Becker, T.W., 2017. The effect of a power-law mantle viscosity on trench retreat rate, *Geophys. J. Int.*, **208**, 491–507.
- Jagoutz, O., Royden, L., Holt, A.F. & Becker, T.W., 2015. Anomalously fast convergence of India and Eurasia caused by double subduction, *Nat. Geosci.*, **8**, 475478, doi:10.1038/ngeo2418.
- Karato, S.I. & Wu, P., 1993. Rheology of the upper mantle—a synthesis, *Science*, **260**(5109), 771–778.
- Kincaid, C. & Griffiths, R.W., 2003. Laboratory models of the thermal evolution of the mantle during rollback subduction, *Nature*, **245**, 58–62.
- Király, A., Capitanio, F., Funiciello, F. & Faccenna, C., 2016. Subduction zone interaction: controls on arcuate belts, *Geology*, **44**(8), doi:10.1130/G37912.1
- Lin, S.C. & Kuo, B.Y., 2016. Dynamics of the opposite-verging subduction zones in the Taiwan region: insights from numerical models, *J. geophys. Res.*, **121**, doi:10.1002/2015JB012784.
- McConnell, R.K., Jr., 1968. Viscosity of the mantle from relaxation time spectra of isostatic adjustment, *J. geophys. Res.*, **73**, 7089–7105.
- McNamara, A.K. & Zhong, S., 2004. Thermochemical structures within a spherical mantle: superplumes or piles?, *J. geophys. Res.*, **109**, doi:10.1029/2003JB002847.
- Mishin, Y.A., Gerya, T.V., Burg, J.P. & Connolly, J.A.D., 2008. Dynamics of double subduction: numerical modeling, *Phys. Earth planet. Inter.*, **171**, 280–295.
- Mitrovica, J.X. & Forte, A.M., 2004. A new inference of mantle viscosity based upon joint inversion of convection and glacial isostatic adjustment data, *Earth planet. Sci. Lett.*, **225**, 177–189.
- Moresi, L.N. & Gurnis, M., 1996. Constraints on the lateral strength of slabs from three-dimensional dynamic flow models, *Earth planet. Sci. Lett.*, **138**, 15–28.
- Piromallo, C., Becker, T.W., Funiciello, F. & Faccenna, C., 2006. Three-dimensional instantaneous mantle flow induced by subduction, *Geophys. Res. Lett.*, **33**, L08304, doi:10.1029/2005GL025390.
- Ribe, N.M., 2010. Bending mechanics and mode selection in free subduction: a thin-sheet analysis, *Geophys. J. Int.*, **180**, 559–576.
- Richards, M.A. & Hager, B.H., 1984. Geoid anomalies in a dynamic Earth, *J. geophys. Res.*, **89**, 5987–6002.
- Royden, L.H. & Husson, L., 2006. Trench motion, slab geometry and viscous stresses in subduction systems, *Geophys. J. Int.*, **167**, 881–895.
- Schellart, W.P., 2004. Quantifying the net slab pull force as a driving mechanism for plate tectonics, *Geophys. Res. Lett.*, **31**(7), doi:10.1029/2004GL019528.
- Schellart, W.P. & Moresi, L., 2013. A new driving mechanism for backarc extension and backarc shortening through slab sinking induced toroidal and poloidal mantle flow: results from dynamic subduction models with an overriding plate, *J. geophys. Res.*, **118**, 3221–3248.
- Schmeling, H. *et al.*, 2008. A benchmark comparison of spontaneous subduction models—towards a free surface, *Phys. Earth planet. Inter.*, **171**, 198–223.
- Stegman, D.R., Farrington, R., Capitanio, F.A. & Schellart, W.P., 2010b. A regime diagram for subduction styles from 3-D numerical models of free subduction, *Tectonophysics*, **483**, 29–45.
- Stegman, D.R., Freeman, J., Schellart, W.P., Moresi, L. & May, D.A., 2006. Influence of trench width on subduction hinge rates in 3-D models of slab rollback, *Geochem. Geophys. Geosyst.*, **7**, doi:10.1029/2005GC001056.
- Stegman, D.R., Schellart, W.P. & Freeman, J., 2010a. Competing influences of plate width and far-field boundary conditions on trench migration and morphology of subducted slabs in the upper mantle, *Tectonophysics*, **483**, 46–57.
- Tan, E., Gurnis, M. & Han, L., 2002. Slabs in the lower mantle and their modulation of plume formation, *Geochem. Geophys. Geosyst.*, **3**(11), 1067, doi:10.1029/2001GC000238.
- Wessel, P., Smith, W.H.F., Scharroo, R., Luis, J. & Wobbe, F., 2013. Generic mapping tools: improved version released, *EOS, Trans. Am. geophys. Un.*, **94**, 409–410.
- Yamato, P., Husson, L., Braun, J., Loiselet, C. & Thieulot, C., 2009. Influence of surrounding plates on 3d subduction dynamics, *Geophys. Res. Lett.*, **36**, doi:10.1029/2008GL036942.
- Zhong, S., 2006. Constraints on thermochemical convection of the mantle from plume heat flux, plume excess temperature and upper mantle temperature, *J. geophys. Res.*, **111**, doi:10.1029/2005JB003972.

SUPPORTING INFORMATION

Supplementary data are available at [GJIRAS](https://doi.org/10.1002/gjras) online.

Supplementary Movies: The supplementary material consists of 3-D animations of each of the double slab configurations, and the reference single slab configuration (Movie 1 = out-dip; Movie 2 = same-dip; Movie 3 = in-dip and Movie 4 = single) with initial slab dip angles of 70° (i.e. models plotted in main Fig. 5). Lithospheric plates are represented by two iso-viscosity contours (one for the lithospheric core and another for the whole lithosphere), with the surfaces coloured by absolute velocity. A horizontal, semi-transparent slice displays the dynamic pressure field at a depth of 400 km. Vectors show the mantle velocity field at depths greater than 150 km, and are plotted with an equivalent scale for each of the animations.

Please note: Oxford University Press is not responsible for the content or functionality of any supporting materials supplied by the authors. Any queries (other than missing material) should be directed to the corresponding author for the paper.